Typeset using LaTeX **twocolumn** style in AASTeX7.0.1

INSIDE EUROPA'S ICE: MODELING SURFACE AND SUB-SURFACE TEMPERATURES

Sydney A. Willis [1], Jordy Bouwman [2,3], Morgan L. Cable [4], Hsiang-Wen Hsu [2], Zoltan Sternovsky [2,5], Henry Cardwell [2,3] and Robin T. Garrod [1,6]

[1] *Department of Chemistry, University of Virginia, Charlottesville, VA 22904, USA*
[2] *Laboratory for Atmospheric and Space Physics, University of Colorado, Boulder, CO 80303, USA*
[3] *Department of Chemistry, University of Colorado, Boulder, CO 80309, USA*
[4] *Planetary Science Institute, Tucson, AZ 85719, USA*
[5] *Smead Aerospace Engineering Sciences Department, University of Colorado, Boulder, CO 80303, USA*
[6] *Department of Astronomy, University of Virginia, Charlottesville, VA 22904, USA*

ABSTRACT

We present a one-dimensional solid-phase heat diffusion model of Europa's ice shell. The model incorporates orbital and physical parameters that influence the surface and sub-surface temperatures, such as Europa's instantaneous distance from the Sun, time of day, local albedo, and internal heating. Europa's surface is divided into 5°×5° latitude-longitude cells, each modeled to a depth of 9.5 km, using 33 depth points distributed to concentrate on the uppermost ice. Each model is run in three stages: the first allowing temperatures at the deepest positions to approach convergence; the second to obtain temperature convergence at all depths; and the third providing high time-resolution data during a cycle of nine orbits of Jupiter around the Sun. These outputs will serve as the thermal profile for planned chemical-kinetic modeling of Europa's ice. Our results suggest a global annual mean surface temperature of 98.5 K, with equatorial temperatures averaging 107.3 K and reaching maxima near 160.0 K, while polar temperatures average ∼55.0 K and reaching minima near 40.6 K. This thermal model will be valuable for interpreting observations of upcoming NASA Europa Clipper and ESA JUICE missions. The model framework is adaptable to other icy moons in our Solar System.

1. INTRODUCTION

The global sub-surface ocean beneath Europa's icy crust makes it one of the most promising places in the Solar System to search for extraterrestrial life (R. T. Pappalardo et al. 1998; M. H. Carr et al. 1998; M. G. Kivelson et al. 2000). It likely contains the key prerequisites for supporting life as we understand it: liquid water, an energy source capable of driving chemical reactions, and a diverse inventory of chemical species (D. J. Des Marais et al. 2008). Many such species—including hydrogen peroxide, sulfur dioxide, and potentially sodium chloride or other salts—have been detected on Europa's surface ice and may be transported into the sub-surface ocean (R. W. Carlson et al. 1999a,b; C. A. Hibbitts et al. 2025; R. Greenberg 2010). Crucially, this potentially habitable sub-surface environment is shielded from Jupiter's intense radiation, providing a stable setting in which complex molecules may survive and undergo further chemical reactions.

It has been proposed that such reactions are driven by the coupled effects of internal heat exchange between Europa's core, ocean, and ice shell, and irradiation of near-surface ice. Together, these processes may play a role in regulating ice thickness and could potentially drive convection or fracturing of the ice shell, facilitating the transport of ocean-derived materials to the surface, as well as the transport of energetically-processed surface materials to the ocean (R. Greenberg 2010).

The potential transport of processed materials to the ocean highlights the importance of understanding the energy sources responsible for the chemical alteration of Europa's surface ice. Solar energetic particles, galactic cosmic rays, ions from Jupiter's magnetosphere, and micrometeorite impacts are all expected to impart energy that may induce chemical changes on or near the surface (R. E. Johnson et al. 2019; J. R. Szalay et al. 2024; S. Kempf et al. 2025). However, comprehensive modeling of these energy sources and their influence on ice chemistry remains limited. Upcoming observations from instruments aboard NASA's Europa Clipper, such as the Surface Dust Analyzer, will give insight into the composition of surface ejecta, constraining the level of energetic processing experienced by the surface (S. Kempf et al. 2025). Chemical models that account for these

Email: swillis@virginia.edu

processes are therefore essential to the interpretation of these observations.

Given the importance of chemical modeling, understanding the thermal regime of the ice shell becomes critical, as temperature controls the rates and pathways of chemical evolution in Europa's ice. Therefore, any computational simulation of the chemical behavior of Europa's surface ice would require information about the temperature structure, ideally as a function of surface-position, depth, and time. The key to understanding Europa's geological activity, diversity of subsurface chemistry, and potential habitability lies in accurately characterizing and modeling the thermal structure of its ice shell (S. D. Vance et al. 2023).

Observations of Europa's thermal emission have provided key constraints on its surface temperature distribution, and previous modeling efforts provide essential insight into Europa's thermal environment, but several aspects of its thermal profile remain insufficiently characterized in the published literature. Existing models can simulate Europa's temperature evolution at specific locations or for selected conditions, yet no study has published a globally consistent, depth- and time-resolved temperature profile. Europa's surface ice exhibits a complex thermal environment, shaped by diurnal and seasonal variations, spatially variable surface properties, and interactions with external energy sources. Capturing this complexity requires a comprehensive thermal model that resolves temperature as a function of both depth and time for the entire surface. Such a dataset is essential for interpreting spatial variability and for integrating realistic thermal structure into multidimensional chemical models.

In this work, we develop a multi-depth thermal model of Europa's ice shell from the surface down to 9.5 km, with a particular emphasis on the temperature structure in the upper 30 m, where energy input from impinging radiation fields and energetic particles may induce chemical activity, to be simulated in follow-up work. Our approach incorporates elements from both Y. Ashkenazy and C. Mergny & F. Schmidt, while introducing our own treatments for parameters such as Jupiter's position in its orbit and its eclipse of Europa. With this model, we produce a spatially-resolved map across latitude and longitude of the time- and depth-dependent temperature across Europa's surface.

The rest of the paper is structured as follows: Sec. 2 describes the thermal model and the parameters affecting Europa's surface temperature. Sec. 3 presents model results as a function of depth and time for a single location, and as a function of latitude and longitude for the entire surface. Sec. 4 compares our results to previous models and discusses the thermophysical and chemical implications. Conclusions are presented in Sec. 5.

2. METHODS

2.1 General Model Setup

We model the temperature of Europa's ice shell in a depth- and time-resolved manner, using a model with vertical heat conduction (i.e., no horizontal conduction). The model is applied independently at various surface positions, allowing the construction of a high-resolution three-dimensional grid of time-dependent temperatures.

Europa's surface is divided into a grid of 5°×5° latitude-longitude cells spanning the entire surface. In the calculations, each cell is represented by the angular midpoint of its longitude-latitude extent; for example, 277.5° W longitude and 12.5° S latitude represent the region from 275-280° W and 10-15° S. However, for simplicity, we label each cell according to the western- and northern-most values for each angle (i.e., 280° W, 10° S, in the example above). This structure results in 2,592 independent, one-dimensional thermal models, with physical parameters evaluated separately for each position.

For every surface position, Europa's ice shell is modeled in a depth-resolved manner, where the ice temperature in each vertical column evolves under a balance of heat gains and losses. Heat gains include insolation at the surface, thermal infrared (IR) radiation from Jupiter, and conductive heat flux from internal heating in the mantle, while heat loss occurs via thermal emission from the surface (see Sec. 2.0.0.0 for details). Although Europa's ice shell is generally thought to be between 15 and 30 km thick (W. B. McKinnon 1999; G. Tobie et al. 2003; S. M. Levin et al. 2026), our model extends only to a depth of 9.5 km. This depth is sufficient to stabilize the effects of internal heating on surface/near-surface temperatures, allowing accurate modeling for the upper ∼30 m of ice. The specific depth positions at which temperatures are calculated through the ice are also chosen to suit the requirements of the planned chemical-kinetic models of those near-surface regions.

Gear's integration algorithm is used to solve the one-dimensional heat transfer equation to 9.5 km depth. A total of 33 depth points are included in the temperature model, representing interfaces between regions of ice through which heat may flow. Temperatures are calculated for each such interface/depth point.

The depth points as well as the separation between each point are listed in Tab. 1. The separation of depth points in the thermal model is chosen based on the planned layer thicknesses in the chemical model, en-

suring high resolution near the surface and increasingly larger layer spacing at greater depths.

The first depth point represents the surface-atmosphere boundary. The second thermal depth point, separated from the first by 2.81×10^{-2} cm, corresponds to the midpoint of what will be the tenth layer in the planned chemical model, which will focus especially on the chemistry very close to the surface. Chemical processing at such depths will be dominated by particles of varying penetration: UV photons reach only a few micrometers, oxygen and sulfur ions penetrate up to a few millimeters, and electrons which can reach up to a few meters (C. Mergny et al. 2025b; C. Paranicas et al. 2002). However, based on test calculations, a resolution of much less than a centimeter is required in the present temperature model, even very close to the surface.

The remaining depth points (3–33) in the thermal model represent the midpoints of each subsequent layer in the chemical model, with the ability to extend to a depth of 10 km. Between ∼8 m and ∼20 m, depth point and layer separation in both models more refined to allow for accurate modeling of the effects of Galactic cosmic rays (GCRs). In our recent chemical models, GCRs are found to be influential to a depth of up to ∼15 m (R. T. Garrod 2019). Thus, the chosen resolution scheme ensures that the temperature gradients relevant to surface chemistry and radiation processing are accurately captured.

In the present model, we consider solar heating and IR thermal heating from Jupiter to be the only external heat sources. Although energetic particles drive radiolytic chemistry in Europa's ice, their energy flux is several orders of magnitude smaller than the insolation at Europa's surface and are therefore negligible in determining surface temperatures. Similarly, micrometeorite impacts provide only sporadic, short-duration energy pulses that are minor compared to insolation. These processes are not considered as energy input in the thermal model.

We carefully account for the time-variation of external heating, which is dependent on both the local position on Europa's surface, and on the overall orbital timing. While sidereal time is used to define the simulation output times and total duration, the synodic day length is employed for calculating the Sun's apparent motion and incoming solar radiation, as described in Sec. 2.3. Jupiter's sidereal orbit around the Sun is 4332.589 Earth days (∼11.87 Earth years), and Europa's sidereal orbit around Jupiter is 3.551 days.[7] However, to ensure exact periodic alignment between Europa's rotation and Jupiter's orbit in the model, we reduce the vales to 4332.578 and 3.550, corresponding to changes of 0.00025% and 0.028%, respectively. This adjustment provides an orbital framework that repeats after precisely nine Jovian years and 10,984 synodic Europa days, providing a manageable period of simulated time, and allowing the resulting temperature profiles to be cycled seamlessly for subsequent chemical modeling whose simulation times (and run-times) are as yet undefined. Each such period of nine adjusted orbits by Jupiter around the Sun, and the associated adjusted orbits of Europa, is referred to hereafter as an "orbital cycle."

[7] https://ssd.jpl.nasa.gov/horizons.cgi

Table 1. Total depth and separation between each point in the heat transfer model.

Depth Point	Total Depth (cm)	Separation (cm)
1	0.00	
2	2.81×10^{-2}	2.81×10^{-2}
3	1.12×10^{-1}	8.43×10^{-2}
4	4.50×10^{-1}	3.37×10^{-1}
5	1.80×10^{0}	1.35×10^{0}
6	7.20×10^{0}	5.40×10^{0}
7	2.88×10^{1}	2.16×10^{1}
8	1.15×10^{2}	8.63×10^{1}
9	4.60×10^{2}	3.45×10^{2}
10	8.05×10^{2}	3.45×10^{2}
11 - 19*	2.05×10^{3}	1.38×10^{2} (×9)
20	2.31×10^{3}	2.60×10^{2}
21	2.75×10^{3}	4.41×10^{2}
22	4.00×10^{3}	1.25×10^{3}
23	2.75×10^{4}	2.35×10^{4}
24	7.50×10^{4}	4.75×10^{4}
25	1.50×10^{5}	7.50×10^{4}
26-33*	9.50×10^{5}	1.00×10^{5} (×8)

NOTE—Depth points represent interfaces between ice layers. Asterisk (*) indicates a group of depth points with the same distance between them; total depth of a group is given as bottom of the final depth point in the group. Layer thickness i corresponds to the interval between depth points $i-1$ and i.

2.2 Orbital Position Calculations

The most influential parameter affecting Europa's surface temperature is its distance from the Sun. Because Europa's orbital distance from Jupiter (∼6.71×10^5 km)[7] is negligible compared to Jupiter's distance from the Sun (∼7.78×10^8 km)[7], we approximate Europa's distance from the Sun simply as Jupiter's heliocentric distance.

To determine Jupiter's instantaneous orbital position and distance from the Sun, we follow Kepler's laws and the standard treatment in C. D. Murray & S. F. Dermott (2000). Each time the solver calculates the temperature, the mean anomaly is calculated from orbital period and time since perihelion. Then, Kepler's equation is solved numerically to obtain the eccentric anomaly, and the true anomaly is computed and used to calculate the instantaneous Sun–Jupiter distance:

$$r = \frac{a(1-e^2)}{1+e\cos\nu}, \tag{1}$$

where a is the semi-major axis, e is the orbital eccentricity, and ν is the true anomaly. This distance feeds directly into the insolation calculation (Eq. 5).

2.3 Heat Diffusion Calculations

To model the evolution of Europa's ice temperatures, we follow the one-dimensional heat diffusion formulation of G. Herman & M. Podolak (1985):

$$\frac{\partial T}{\partial t} = \kappa \frac{\partial^2 T}{\partial z^2}, \tag{2}$$

where T is temperature, z is depth, t is time, and κ is the thermal diffusivity of ice.

The upper boundary condition accounts for incoming solar radiation, thermal IR radiation from Jupiter, and outgoing thermal emission. Following the methods of Y. Ashkenazy (2019), we define the upper boundary condition as:

$$\rho_I c_I \kappa_s \frac{\partial T_s}{\partial z} = W(1-\alpha)(1-p) + W_j - \epsilon\sigma T_s^4, \tag{3}$$

where ρ_I and c_I are the density and heat capacity of the ice, κ_s is the surface ice diffusivity, W is insolation (Eq. 5), α is albedo, p is the eclipse fraction, W_j is radiation from Jupiter, ϵ is emissivity, and σ is the Stefan–Boltzmann constant.

The lower boundary includes internal heating, and also follows Y. Ashkenazy (2019):

$$\rho_I c_I \kappa_d \frac{\partial T}{\partial z} = -Q, \tag{4}$$

where κ_d is the diffusivity of the deep ice and Q is the internal heat flux.

Insolation at Europa is given by A. Berger et al. (1993):

$$W = S_0 \left(\frac{a}{r}\right)^2 \cos\theta_s, \tag{5}$$

where S_0 is the solar constant at Jupiter, a is the semi-major axis, r is the instantaneous Sun–Jupiter distance (Eq. 1), and θ_s is the solar zenith angle:

$$\cos\theta_s = \sin\phi_e \sin\delta + \cos\phi_e \cos\delta \cos H_{syn}, \tag{6}$$

with ϕ_e as latitude on Europa, δ the declination angle, and H_{syn} the hour angle based on the synodic day. Here, H_{syn} is calculated from the sidereal time (T_{sid}) to account for Europa's orbital motion around Jupiter relative to the Sun:

$$H_{syn} = T_{sid} - \lambda_e - \nu, \tag{7}$$

where λ_e is Europa's surface longitude and ν is Jupiter's true anomaly. This ensures that the incoming solar radiation correctly reflects the daily and seasonal cycles observed on Europa.

The angle δ is related to obliquity ε and true longitude λ_j:

$$\sin\delta = \sin\varepsilon \sin\lambda_j, \tag{8}$$

and the true longitude is related to the true anomaly ν and Jupiter's longitude of perihelion $\bar{\omega}$ by

$$\lambda_j = \nu + \bar{\omega}. \tag{9}$$

Thermal IR radiation from Jupiter is also included. Unlike Y. Ashkenazy (2019), who assume hemispherically uniform flux, we calculate longitude–latitude dependence for Europa's sub-Jovian hemisphere:

$$W_j = J_0 \cos\phi_e \cos\lambda_e, \tag{10}$$

where J_0 is Jupiter's radiation constant. On the anti-Jovian hemisphere, W_j is set to zero.

2.4 Explanation of Chosen Parameter Values

To model Europa's surface temperature over the annual and diurnal cycles, the parameters referenced in Eqs. 1–10 and listed in Tab. 2 are incorporated into the model. Parameters requiring further explanation are marked there with a special character and are described below.

2.4.1 Orbital Parameters

We adopt a mean obliquity of 3° for Europa (ε), following Y. Ashkenazy (2019), which accounts for Europa's axial tilt, Jupiter's tilt, and Europa's orbital inclination. This value has a negligible effect on global and equatorial temperatures, with only a minor (∼1.8 K) increase at the poles compared to slightly higher obliquities (Y. Ashkenazy 2019).

Europa experiences periodic eclipses by Jupiter, during which solar radiation is blocked. A simple treatment for this effect is to adjust the total insolation for regions that are affected by the eclipse. Because Europa

Table 2. Physical parameters used in the calculation of heat diffusion on Europa.

Parameter & Description	Value
ε Europa's obliquity*	3°
p time in Jupiter's shadow*	variable
e Jupiter's eccentricity*	0.0487
$\bar{\omega}$ Jupiter's longitude of perihelion*	14.75385°
ϵ Europa's emissivity†	0.9
α bolometric albedo of Europa†	variable
κ_s surface ice thermal diffusivity†	7.7×10^{-6} cm^2/s
κ_d deep ice thermal diffusivity†	1.54×10^{-2} cm^2/s
ρ_I density of ice	9.17×10^{-1} g/cm^3
c_I specific heat of ice	2.0×10^{7} erg/g/K
Q internal heating rate‡	10 erg/s/cm^2
S_0 solar constant at Jupiter	5.10×10^{4} erg/s/cm^2
J_0 Jupiter's radiation constant	1.76×10^{2} erg/s/cm^2

Parameters requiring more explanation are indicated by a special character: asterisk (*) for orbital parameters, (†) for surface and ice properties, and (‡) for internal heating.

is tidally locked, only the sub-Jovian hemisphere (0–90° W and 270–360° W) is affected, while the anti-Jovian hemisphere (90–270° W) experiences nighttime (i.e., no incoming solar radiation) during the eclipse. Following Y. Ashkenazy (2019), we approximate the fraction of time spent in Jupiter's shadow as p. Unlike Y. Ashkenazy (2019), who apply $p = 0.033$ globally, we apply this value only to the sub-Jovian hemisphere, and use $p = 0.0$ for the anti-Jovian hemisphere, providing a simple treatment of this effect in the heat diffusion calculations (Eq. 3).

2.4.2 Surface and Ice Properties

The bolometric albedo, also called the Bond albedo, is defined as the fraction of incident solar energy reflected across all wavelengths. The values we use are based on the high-resolution map of C. Mergny et al. (2025a), derived from USGS Voyager and Galileo photometric data. For use in the thermal model, the map was rebinned and averaged into 5° × 5° latitude-longitude cells, matching the spatial structure of the model grid. The high-resolution map from C. Mergny et al. lacks data for some areas in the south polar region due to limited thermal imaging observations below 83° S. To avoid missing values, we filled the south polar albedo data with the nearest available value along the same longitude.

We adopt a global bolometric (i.e., across all wavelengths) emissivity of 0.9 for Europa, consistent with J. A. Rathbun et al. (2010) and S. K. Trumbo et al. (2018). Spatial variations in surface morphology are not incorporated due to a lack of comprehensive emissivity data across Europa.

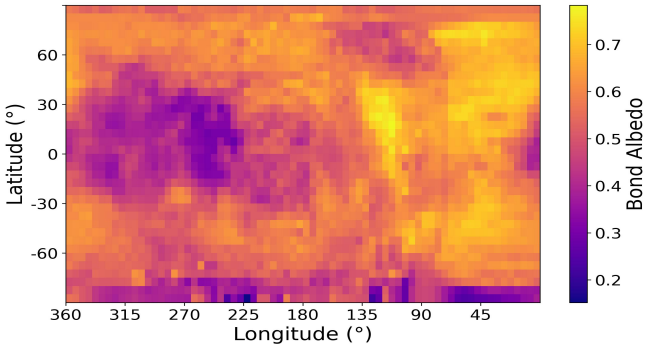

Figure 1. Low-resolution Bond albedo map of Europa's surface derived from C. Mergny et al. (2025a). Note: south polar values are extrapolated from incomplete data to give a complete map.

Thermal diffusivity (κ) determines how quickly a material responds to heating. For Europa's deep ice, we adopt $\kappa_d = 1.54 \times 10^{-2}$ cm^2 s^{-1}, consistent with crystalline water ice (R. L. Kirk & D. J. Stevenson 1987; H. Hussmann et al. 2002; M. Beuthe 2015). Surface ice is expected to have a lower diffusivity due to porosity, grain size, and ion bombardment effects (A. E. Thelen et al. 2024), with typical values ranging from 9.0×10^{-6} to 1.0×10^{-4} cm^2 s^{-1}. We use $\kappa_s = 7.7 \times 10^{-6}$ cm^2 s^{-1} (Y. Ashkenazy 2019) for the first 6 depth points, representing the upper 7.20 cm of the ice. This value also falls within the error range of thermal diffusivities converted from Atacama Large Millimeter/submillimeter Array (ALMA) Band 6 thermal inertia measurements, which probe between 1.5 and 3.0 cm (A. E. Thelen et al. 2024).

2.4.3 Internal Heating of Europa

Europa's internal heating is poorly constrained but likely arises from a combination of tidal deformation and the resulting dissipative heating in the core, subsurface ocean, and ice shell, as well as radiogenic heating in the rocky core (G. Tobie et al. 2003; F. Nimmo et al. 2007; G. Tobie et al. 2025). While some studies neglect internal heating due to its small contribution relative to solar flux (C. Mergny & F. Schmidt 2024), it can have a greater effect at the poles where insolation is low (Y. Ashkenazy 2019). Furthermore, because our model extends to 9.5 km depth, internal heating contributes to the thermal profile at these depths. To account for this, we include a uniform internal heating rate of $Q = 10$ erg s^{-1} cm^{-2}, slightly lower than Y. Ashkenazy (2019), but in agreement with deep ice heat flux from G. Tobie et al. (2003).

2.4.4 Model Execution and Convergence

Because of the large depth of the modeled ice shell, the thermal model is run in three stages. The purpose of the first stage is to allow the deepest depth points, which are insensitive to diurnal or seasonal fluctuations, to converge under the influence of internal heating (Sec. 2.4.3). To do this, the model is initialized at a uniform temperature of 95 K for every position. During this stage, the solar flux at the surface is not calculated as a function of distance from the Sun, but is applied as an average yearly value for each 5° latitude cell, and no orbital variations are included. Temperatures are output every 3.0672×10^{10} sec (i.e., on timescales much longer than Jupiter's sidereal orbital period), and the stage is considered converged once the difference between successive outputs is less than 10^{-2} K at all depths for two consecutive outputs. The simulated time it takes to reach this criterion is roughly one billion years for each position.

The second stage focuses on achieving temperature convergence across consecutive orbital cycles for the upper depth points, which are sensitive to both diurnal and seasonal variations. This stage is initiated using the final temperature profiles of stage 1 as input, and incorporates time-dependent solar radiation, as described in Sec. 2.2, based on both the orbital position of Europa and the geographical position on Europa's surface. Model runs are carried out over multiples of the orbital cycle. The final profile from each cycle is used as the starting point for the next, and iterations continue until temperatures at all depths differ by less than 10^{-2} K between consecutive cycle end-points. Convergence takes between 50 and 600 orbital cycles, depending on the position.

In the third and final stage, the fully converged model is run for a single orbital cycle at high temporal resolution, providing temperature outputs every 4260 seconds (i.e. 72 times per Europa day). The final temperatures from stage 2 are used as initial temperatures in this stage. This resolution captures the full diurnal cycle at each location and allows maximum and minimum daily surface temperatures to be identified.

3. RESULTS

Using the data from the one-dimensional heat transfer model, we calculate Europa's average surface temperatures and insolation for various regions across Europa's surface (Tab. 3). The global average surface temperature, computed as the annual average of a diurnal period, is 98.5 K, and the average insolation at Europa, again computed as the annual average of diurnal periods is 10,229 erg s^{-1} cm^{-2}. The equatorial region experiences the highest levels of insolation, and therefore reaches higher temperatures than other regions on the surface.

Table 3. Average yearly values for global regions.

Region	Range	Temp (K)	Insolation (erg/s/cm^2)	Bond Albedo
Global	all	98.5	10,228	0.549
Equatorial	5° N–5° S	107.3	12,763	0.500
N. Polar	85° N–90° N	52.4	1,009	0.562
S. Polar	85° S–90° S	56.1	1,009	0.399
Leading	0–180° W	95.5	10,228	0.609
Trailing	180–360° W	101.4	10,228	0.489
Sub-Jovian	270–90° W	97.8	9,891	0.559
Anti-Jovian	90–270° W	99.1	10,558	0.540

Regional averages were computed from all grid points within the indicated latitudinal or longitudinal ranges.

The leading and trailing hemispheres receive the same level of solar insolation, but their average temperatures are 93.7 K and 99.5 K, respectively. This difference is a result of the bolometric albedo values for each region. The higher albedo of the leading hemisphere means that more radiation is reflected from its surface, resulting in less absorption of energy as heat, and therefore lower temperatures. A similar, but less extreme albedo effect is seen in the difference in the average temperatures of the sub-Jovian and anti-Jovian hemispheres, where the sub-Jovian hemisphere has a higher albedo and a lower average temperature. However, this temperature difference can also be attributed, in part, to Jupiter's eclipse of Europa, with only the sub-Jovian hemisphere experiencing this effect.

The polar regions, which receive very little solar radiation, have much lower temperatures than equatorial regions. The north and south polar regions average temperatures of 49.2 K and 52.9 K, respectively. The difference between polar temperatures largely reflects local bolometric albedo differences, as the north pole has a higher average albedo (0.562) than the south pole (0.399); note that south polar values are extrapolated from incomplete data, and the results from the south polar region should be interpreted with caution.

Maximum yearly surface temperatures at each 5°×5° grid point are shown in Fig. 2. These temperatures do not represent values across the entire surface at a single point in time, but rather are the maximum temperatures reached at any time during a single orbital cycle. Comparing this temperature map to the bolometric albedo map in Fig. 1, it is clear that the surface temperature is influenced greatly by the bolometric albedo. Similar patterns can been seen in the albedo

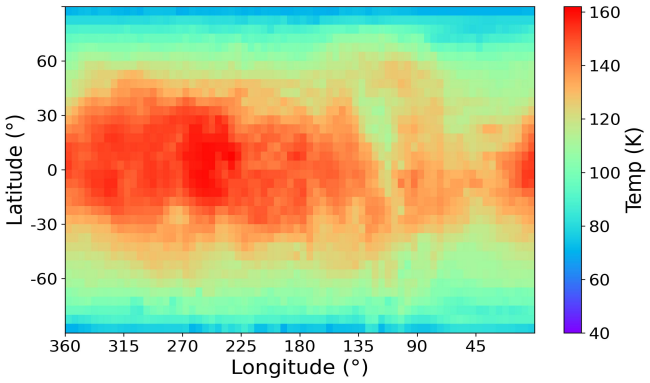

Figure 2. Maximum surface temperatures reached during a single orbital cycle calculated by the one-dimensional heat transfer model at 5°×5° resolution across Europa. Color bars use the same scale to more clearly show difference between average, maximum, and minimum temperatures.

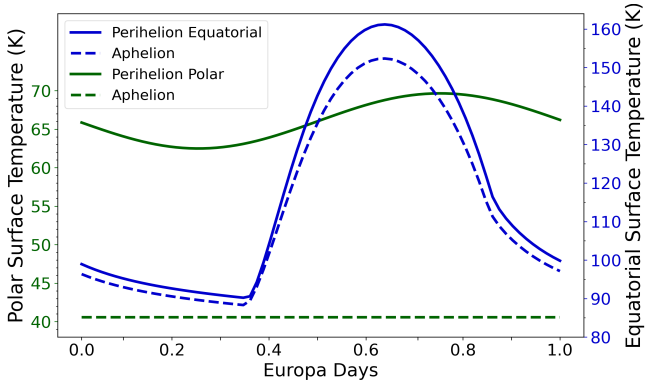

Figure 3. Surface temperature for two positions, each shown near perihelion and aphelion. The equatorial position corresponds to 235° W, 10° S, which experiences hottest diurnal temperature. The polar position corresponds to 160° W, 90° N, which experiences the coldest diurnal temperature.

and temperature maps, where regions of lower albedo correspond to regions of higher temperature. For example, the Pwyll Crater region (271° W, 25° S (J. M. Moore et al. 1998)), which is represented in our maps by the grid cell 270° W, 25° S, is characterized by higher albedo than the surrounding area, resulting in the lower maximum temperatures seen in Fig. 2. The strong influence of albedo on surface temperature is consistent with previous studies investigating albedo-temperature relationships (H. H. Kieffer 2013; P. R. Christensen et al. 2024).

These global trends are reflected in the locations of the extreme daytime temperatures during a diurnal cycle. The highest daytime temperature of 158.7 K occurs at (235° W, 10° N), shown in Fig. 3. This site lies near the equator on the anti-Jovian hemisphere, and coincides with the lowest albedo (0.279), resulting in enhanced solar absorption and increased temperatures. In contrast, the lowest daytime temperature of 40.6 K occurs at (160° W, 90° N), near the north pole where the high albedo (0.603) severely limits solar heating (Fig. 3).

Having identified these extreme locations, Fig. 3 illustrates how their surface temperatures vary over a diurnal cycle at two points, perihelion and aphelion, in Europa's orbit. The equatorial location exhibits diurnal temperature fluctuations of ∼70 K during warmest periods (i.e., perihelion), and ∼60 K during colder periods near (i.e., aphelion). In contrast, the polar region shows a diurnal variation of only ∼6 K during warm periods and almost no fluctuation during cold periods.

To illustrate how surface temperature fluctuations propagate downward at a single position, Fig. 4 shows the temperature evolution over one Europa day at five different sub-surface depths. This snapshot is taken just after perihelion, when the location reaches its maximum

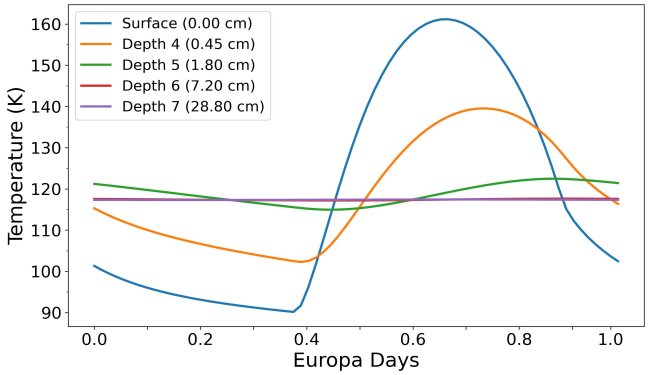

Figure 4. Surface temperature as a function of depth at 235° W, 10° S, just after perihelion. The surface depth has no thickness, and corresponds to the surface-atmosphere interface.

temperature during the orbital cycle. The surface experiences the largest diurnal fluctuation, responding directly to variations in insolation, while the amplitude of temperature variations decreases with depth. At depths between 7.20 cm and 28.80 cm the temperatures remain nearly constant, demonstrating the damping of diurnal signals at greater depths. The time of peak temperature at each depth shifts later with increasing depth, demonstrating the lag of heat transfer through the ice.

4. DISCUSSION

The thermal model developed in this work predicts an equatorial annual mean temperature of 107.3 K, which agrees very well with the equatorial seasonal temperature of 106 K predicted by J. R. Spencer et al. (1999) (see Sec. 3). The predicted global annual mean surface temperature is 98.5 K, which is higher than the global mean temperature of 90.1 K reported by Y. Ashkenazy

(2019). Several factors likely contribute to this difference.

One contributing factor is our use of location-specific albedo values derived from C. Mergny et al. (2025a). After re-binning and averaging, these data yield a global mean albedo of value 0.549, compared to global value of 0.6 adopted by Y. Ashkenazy (2019). The higher albedo assumed in their model therefore leads to a lower predicted global mean temperature.

Additionally, in this work, we perform a full thermal analysis for each of the 2,592 surface positions and calculate the global and regional mean temperatures by area-weighted averaging. However, Y. Ashkenazy (2019) calculate the annual temperatures for each region using a mean annual insolation value for that region. Furthermore, our treatment of Europa's eclipse by Jupiter increases the mean insolation for anti-Jovian longitudes compared to the treatment of Y. Ashkenazy (2019), providing another possible contributor to the differences in reported global and regional mean temperatures.

Our model also provides a depth- and time-dependent view of Europa's entire surface and ice temperature, offering a unique understanding of how Europa's orbital dynamics and thermal properties affect the temperature of the ice shell. By explicitly resolving diurnal temperature and sub-surface structure, the model captures both the immediate effects of insolation and the delayed response due to heat capacity and thermal diffusivity.

Fig. 5 provides a cartographic view of how Europa's entire surface temperature evolves over a single diurnal cycle, shown at four times (0.25, 0.5, 0.75, and 1.0 Europa days). The white dashed lines indicate the longitude of peak instantaneous solar radiation (local solar noon), shown on the leading hemisphere of the first column and the trailing hemisphere of the third column. Although these lines trace the progression of maximum insolation as Europa rotates, the warmest surface temperatures do not always coincide spatially with this longitude.

For example, in the first column, the hottest region occurs at (95° W, 10° S), even though this location has not yet reached local solar noon. This is likely a result of the relatively low albedo of this area (∼0.527) compared to nearby regions such as (90° W, 10° S), which has a slightly higher albedo (∼0.586). The lower albedo allows the surface to retain more solar energy, causing it to reach higher temperatures earlier in the day than the adjacent higher-albedo areas.

In the third column, the hottest region has already passed local solar noon, but it remains warmer than nearby locations that are currently at peak insolation. This behavior reflects both the albedo differences and the heat capacity of the ice. Because the hottest region has a lower albedo, it absorbs more energy, and the finite heat capacity of the ice causes the stored heat to be released later in the day, so surface temperatures peak after maximum insolation.

Thermal models and observations are inherently complementary: models provide the framework for interpreting observational data, while well-constrained models rely on observations to validate and refine their results. Therefore, Europa Clipper will both test and refine our thermal model predictions.

In particular, the Europa Thermal Emission Imaging System (E-THEMIS) is an infrared camera that is designed to map the brightness temperature of Europa's surface (P. R. Christensen et al. 2024). By providing multi-time or multi-wavelength observations of Europa, E-THEMIS will help constrain key surface properties such as thermal inertia Γ, albedo α and surface roughness.

The Mapping Imaging Spectrometer for Europa (MISE) will provide imaging data with spectroscopic data to link the composition of Europa with its physical properties such as albedo and emissivity (D. L. Blaney et al. 2024). Collectively, the data provided by these instruments and others on Europa Clipper will reduce uncertainties in the model inputs, improve interpretation of observed surface properties and enable more confident model-based predictions. This capability is especially important for regions with limited observational coverage such as polar regions. A well-calibrated thermal model can thus be used to predict conditions in these poorly observed areas and guide future observations.

5. CONCLUSIONS

Europa's sub-surface ocean and overlying ice shell remain among the most compelling targets for astrobiological and astrochemical exploration because of the unique conditions provided by the energetic coupling of these two environments. The high level of scientific interest is evidenced by NASA's Europa Clipper and ESA's JUICE mission, both designed to characterize Europa's ice shell and investigate Europa's potential habitability.

In advance of these missions, thermal modeling is essential for interpreting previous observations and predicting how the thermal profile will affect chemical processes. In this work, we developed a depth- and time-dependent thermal diffusion (heat transfer) model for Europa's ice shell. We used our model to predict the thermal profile of Europa's entire surface and its subsurface ice to a depth of 9.5 km. We summarize the main conclusions below:

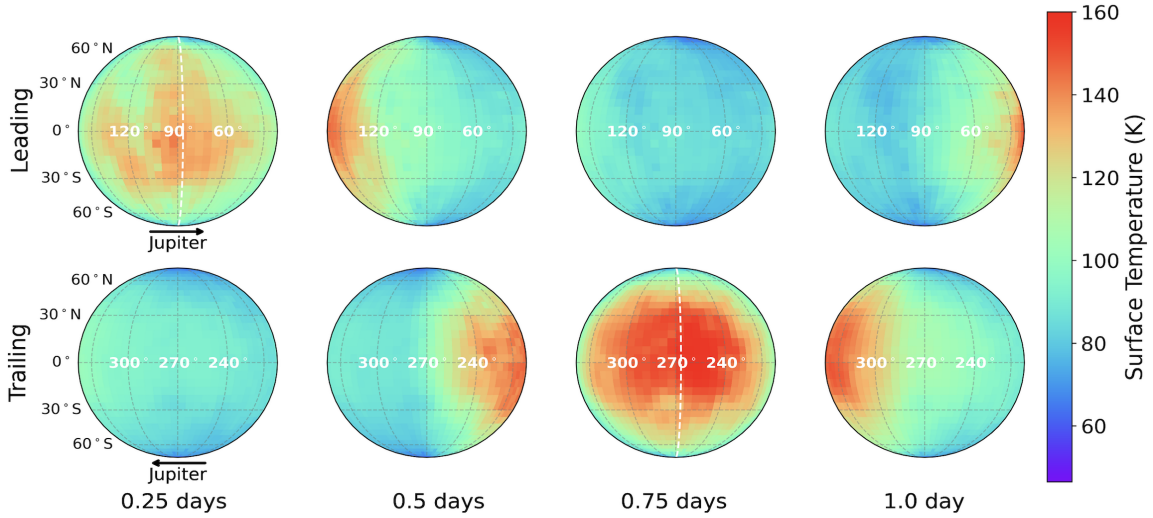

Figure 5. Modeled surface temperature of Europa at four time points in a single Europa day at perihelion, when insolation is highest. Warmer regions are shown in red, and cooler regions are shown in blue, according to the color bar. The white dashed lines in the first and third panels correspond to local solar noon times. Black arrows indicate the direction toward Jupiter. Time snapshots are shown in columns, corresponding to 0.25 days, 0.5 days, 0.75 days and 1.0 days. The leading hemisphere is always shown in the top row, and the trailing hemisphere is always shown in the bottom row. Latitude labels are shown only on the leftmost plots, and longitude labels are indicated along the equator and are given in W longitude.

1. Our predicted global mean surface temperature on Europa of 96.6 K refines previous estimates by incorporating spatially resolved albedo values, rather than a globally uniform assumption. However, the accuracy of this refinement remains limited by the available albedo coverage, particularly at polar regions where additional observations could further improve the model.

2. The use of the spatially varied albedo values highlights the strong influence that local bolometric albedo exerts on Europa's surface temperatures. Both diurnal and annual temperature maps show a clear correlation between lower-albedo regions reaching higher temperatures and higher-albedo regions remaining cooler.

3. Analysis of the vertical temperature structure indicates that Europa's diurnal temperature variations are confined to only a few centimeters into the ice shell, converging to a stable profile between 3 and 12 cm, based on our depth resolution.

Thermal models such as the one developed in this work will be essential tools for interpreting observations from Europa Clipper, JUICE, and other ground- and space-based measurements. Our model is unique because it not only captures depth- and time-dependent temperature structure but it also allows for more precise position-specific predictions. By adjusting local parameters such as albedo, emissivity, and diffusivity, the model can be tailored to individual positions and used to explore how these properties affect the temperature.

Although this work is focused on the thermal modeling of Europa, our ultimate goal is to model the chemistry in its near-surface ice. Chemical models require explicit depth and time-dependent temperatures over long, continuous time-scales. This level of detail is not possible to obtain from observations. Thus, thermal models will remain essential for capturing the full, continuous temperature structure of the ice shell, regardless of improvements in observations. As new observations provide finer constraints, the model can be refined to improve accuracy and deepen our understanding of Europa's ice thermal structure.

Finally, this model can also be applied to other icy moons in our solar system, including Saturn's moons Enceladus and Titan, as well as Jovian moons Ganymede and Callisto. Adapting the model to these worlds would require only modest adjustments to account for their different orbital and surface properties. Such extensions are timely given upcoming missions like JUICE and the continued interest in Enceladus as a high-priority astrobiology target (G. Mitri et al. 2022).

ACKNOWLEDGMENTS

The material is based upon work supported by NASA under the Precursor Science Investigations for Europa (PSI-E) program (award number 80NSSC24K0401). S. Willis also acknowledges support from VSGC. We thank

P. Arras for helpful discussions on the orbital mechanics of Europa. We also thank C. Mergny for providing the albedo data and for valuable discussions regarding the effects of thermal inertia.

REFERENCES

Ashkenazy, Y. 2019, Heliyon, 5:e01908, doi: 10.1016/j.heliyon.2019.e01908

Berger, A., Loutre, M.-F., & Tricot, C. 1993, J. Geophys. Res., 98, 10341, doi: 10.1029/93JD00222

Beuthe, M. 2015, Icarus, 248, 109, doi: 10.1016/j.icarus.2014.10.027

Blaney, D. L., Hibbitts, K., Diniega, S., et al. 2024, SSRv, 220, 80, doi: 10.1007/s11214-024-01097-8

Carlson, R. W., Johnson, R. E., & Anderson, M. S. 1999a, Science, 286, 97, doi: 10.1126/science.286.5437.97

Carlson, R. W., Anderson, M. S., Johnson, R. E., et al. 1999b, Science, 283, 2062, doi: 10.1126/science.283.5410.2062

Carr, M. H., Belton, M. J. S., Chapman, C. R., et al. 1998, Nature, 391, 363, doi: 10.1038/34857

Christensen, P. R., Spencer, J. R., Mehall, G. L., et al. 2024, SSRv, 220, 38, doi: 10.1007/s11214-024-01074-1

Des Marais, D. J., Nuth, III., J. A., Allamandola, L. J., et al. 2008, Astrobiology, 8, 715, doi: 10.1089/ast.2008.0819

Garrod, R. T. 2019, ApJ, 884, 69, doi: 10.3847/1538-4357/ab418e

Greenberg, R. 2010, Astrobiology, 10, 275, doi: 10.1089/ast.2009.0386

Herman, G., & Podolak, M. 1985, Icarus, 61, 252, doi: 10.1016/0019-1035(85)90107-1

Hibbitts, C. A., Stockstill-Cahill, K., Lloyd, E., et al. 2025, PSJ, 6, 282, doi: 10.3847/PSJ/ae182c

Hussmann, H., Spohn, T., & Wieczerkowski, K. 2002, Icarus, 156, 143, doi: 10.1006/icar.2001.6776

Johnson, R. E., Oza, A. V., Leblanc, F., et al. 2019, SSRv, 215, 20, doi: 10.1007/s11214-019-0582-1

Kempf, S., Tucker, S., Altobelli, N., et al. 2025, SSRv, 221, 10, doi: 10.1007/s11214-025-01134-0

Kieffer, H. H. 2013, Journal of Geophysical Research (Planets), 118, 451, doi: 10.1029/2012JE004164

Kirk, R. L., & Stevenson, D. J. 1987, Icarus, 69, 91, doi: 10.1016/0019-1035(87)90009-1

Kivelson, M. G., Khurana, K. K., Russell, C. T., et al. 2000, Science, 289, 1340, doi: 10.1126/science.289.5483.1340

Levin, S. M., Zhang, Z., Bolton, S. J., et al. 2026, Nature Astronomy, 10, 84, doi: 10.1038/s41550-025-02718-0

McKinnon, W. B. 1999, Geophys. Res. Lett., 26, 951, doi: 10.1029/1999GL900125

Mergny, C., & Schmidt, F. 2024, PSJ, 5, 215, doi: 10.3847/PSJ/ad6d6e

Mergny, C., Schmidt, F., Andrieu, F., & Belgacem, I. 2025a, A&A, 693, L21, doi: 10.1051/0004-6361/202453058

Mergny, C., Schmidt, F., & Keil, F. 2025b, Icarus, 441, 116700, doi: 10.1016/j.icarus.2025.116700

Mitri, G., Barnes, J., Coustenis, A., et al. 2022, Experimental Astronomy, 54, 877, doi: 10.1007/s10686-021-09772-2

Moore, J. M., Asphaug, E., Sullivan, R. J., et al. 1998, Icarus, 135, 127, doi: 10.1006/icar.1998.5973

Murray, C. D., & Dermott, S. F. 2000, The Two-Body Problem (Cambridge University Press), 22–62

Nimmo, F., Thomas, P. C., Pappalardo, R. T., & Moore, W. B. 2007, Icarus, 191, 183, doi: 10.1016/j.icarus.2007.04.021

Pappalardo, R. T., Head, J. W., Greeley, R., et al. 1998, Nature, 391, 365, doi: 10.1038/34862

Paranicas, C., Ratliff, J. M., Mauk, B. H., Cohen, C., & Johnson, R. E. 2002, Geophys. Res. Lett., 29, 1074, doi: 10.1029/2001GL014127

Rathbun, J. A., Rodriguez, N. J., & Spencer, J. R. 2010, Icarus, 210, 763, doi: 10.1016/j.icarus.2010.07.017

Spencer, J. R., Tamppari, L. K., Martin, T. Z., & Travis, L. D. 1999, Science, 284, 1514, doi: 10.1126/science.284.5419.1514

Szalay, J. R., Allegrini, F., Ebert, R. W., et al. 2024, Nature Astronomy, 8, 567, doi: 10.1038/s41550-024-02206-x

Thelen, A. E., de Kleer, K., Camarca, M., et al. 2024, PSJ, 5, 56, doi: 10.3847/PSJ/ad251c

Tobie, G., Auclair-Desrotour, P., Běhounková, M., et al. 2025, SSRv, 221, 6, doi: 10.1007/s11214-025-01136-y

Tobie, G., Choblet, G., & Sotin, C. 2003, Journal of Geophysical Research (Planets), 108, 5124, doi: 10.1029/2003JE002099

Trumbo, S. K., Brown, M. E., & Butler, B. J. 2018, AJ, 156, 161, doi: 10.3847/1538-3881/aada87

Vance, S. D., Craft, K. L., Shock, E., et al. 2023, SSRv, 219, 81, doi: 10.1007/s11214-023-01025-2